Supplementary Information

Tuning Porous $Li_{6.25}Ga_{0.25}La_3Zr_2O_{12}$ (LGLZO) Frameworks for Enhanced Ion Transport in Semi-Solid-State Lithium Metal Batteries

Ziyao Wang[a], Sijia Huo [a,*], Meichen Pan[a], Yihan Qiu [a], Ying Tian [a], Ying Zhou [a], Wei Yan [a], Xiaoming Duan [a], Wen Wang [a,*], Yu Zhou [a]

[a] Harbin Institute of Technology, School of Materials Science and Engineering, Harbin 150001, China

* Corresponding author.

E-mail: wangwen@hit.edu.cn(W. Wang) and huosijia@hit.edu.cn (S. Huo)

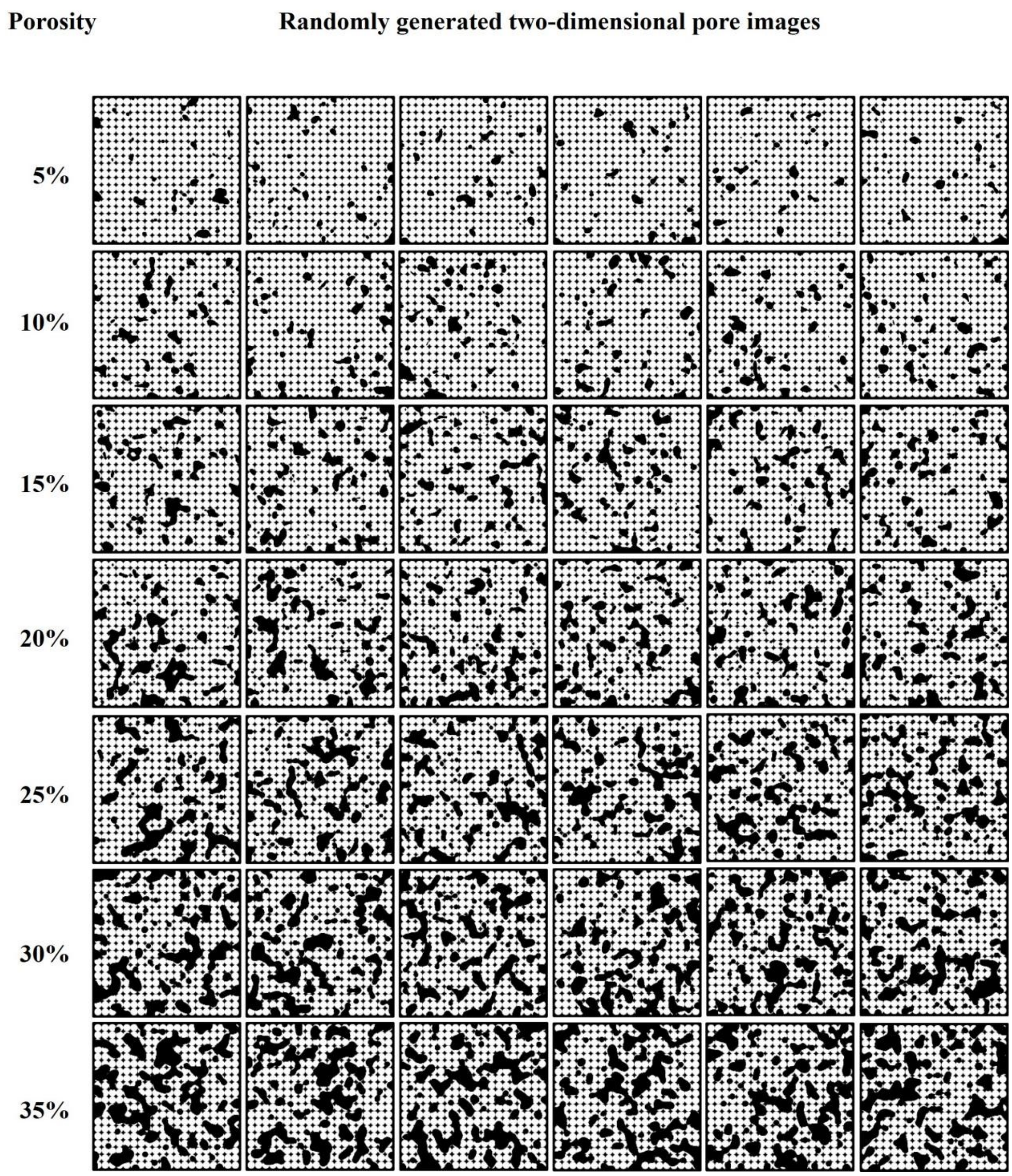

Figure S1. Randomly generated two-dimensional pore structures with porosity ranging from 5% to 35%, where the black regions represent pores and the white regions correspond to the LGLZO framework.

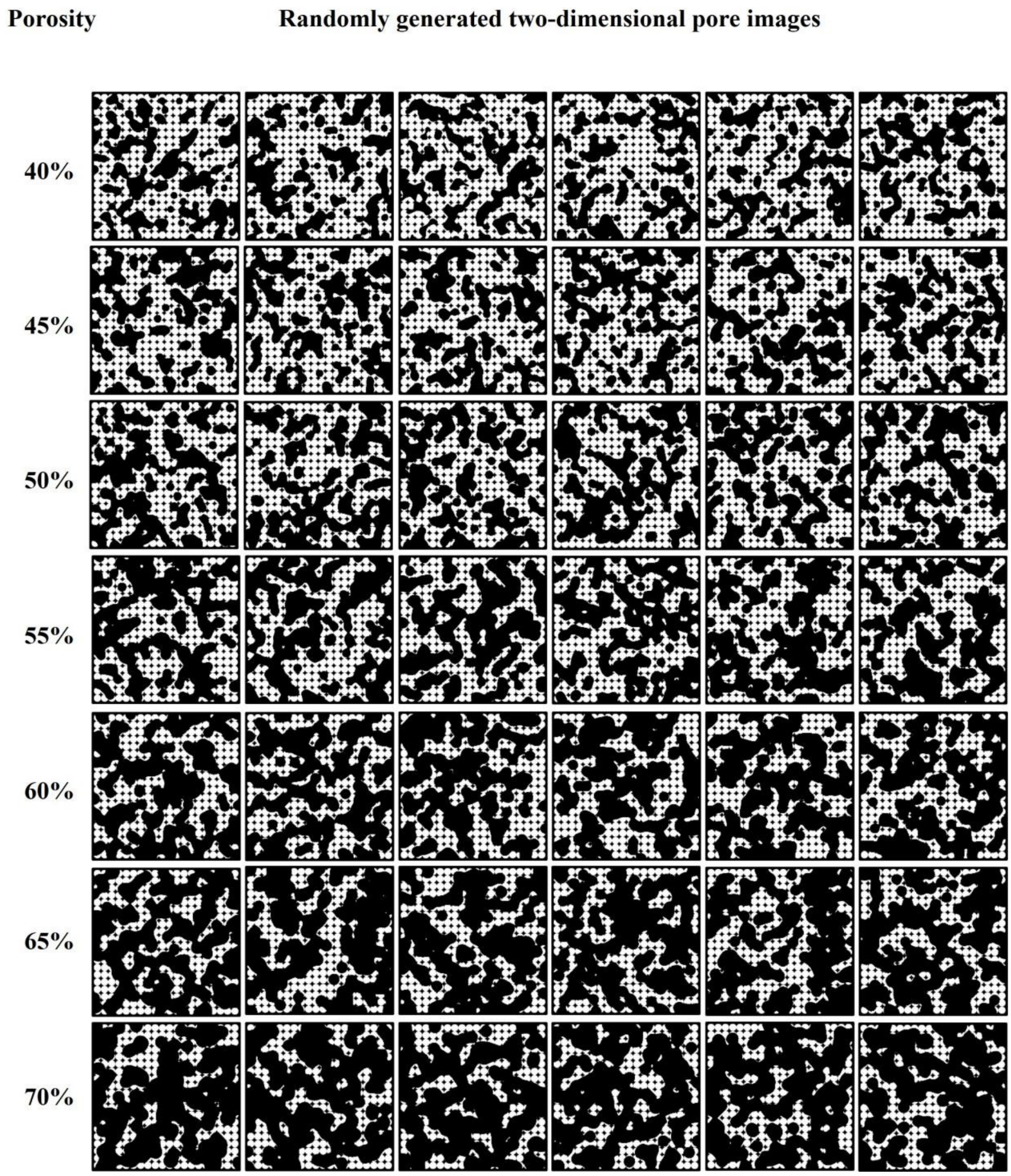

Figure S1. Randomly generated two-dimensional pore structures with porosity ranging from 40% to 70%, where the black regions represent pores and the white regions correspond to the LGLZO framework.

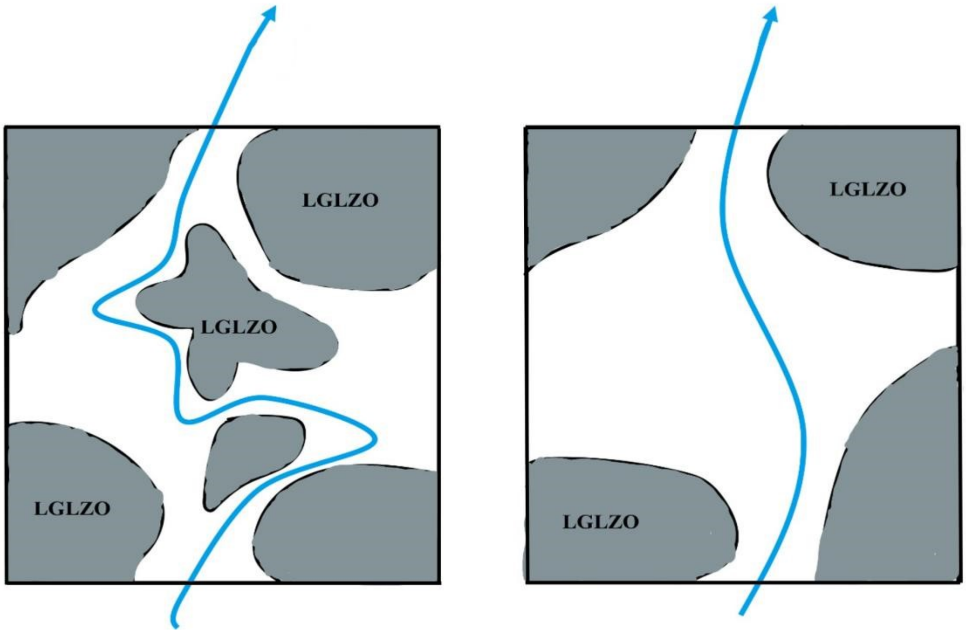

Figure S2. Schematic illustration of lithium-ion migration in different pore structures.

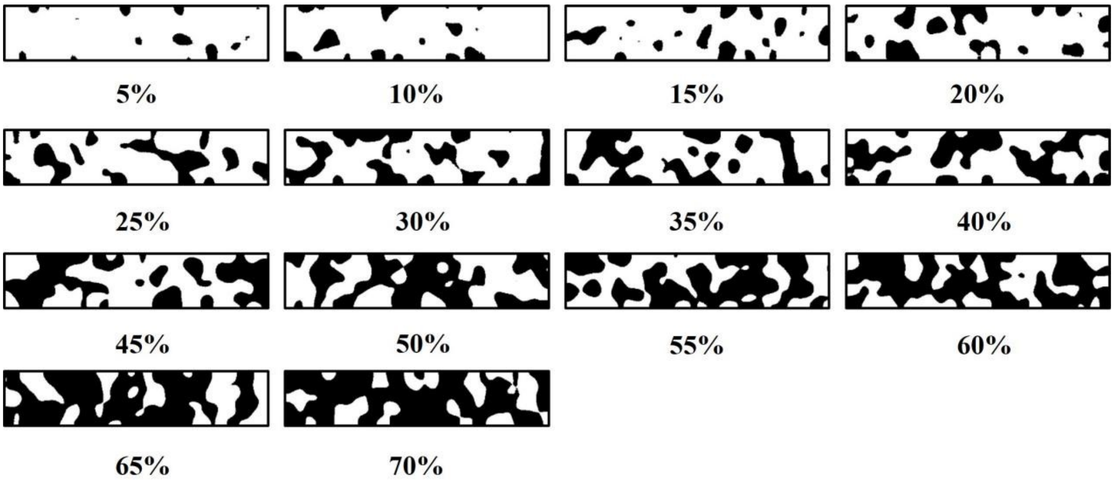

Figure S3. Two-dimensional images (100 dpi × 500 dpi) of porous structures with porosity ranging from 5% to 70%.

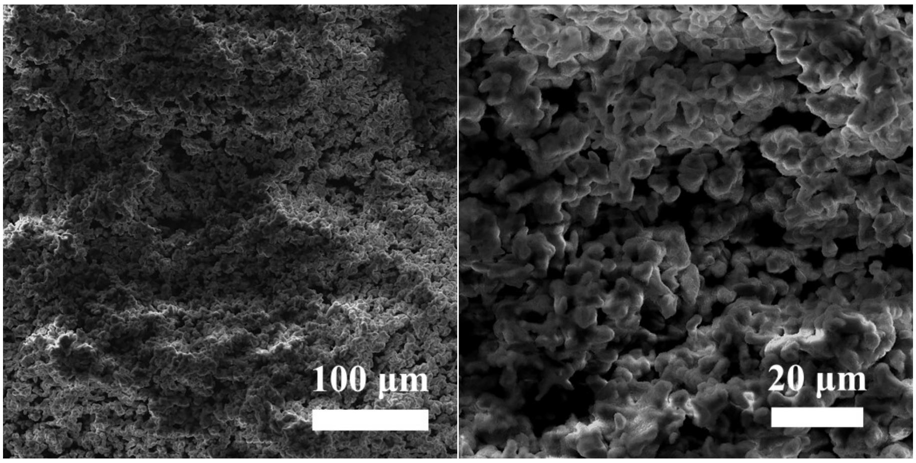

Figure S4. LGLZO green body after calcination for carbon removal and before sintering.

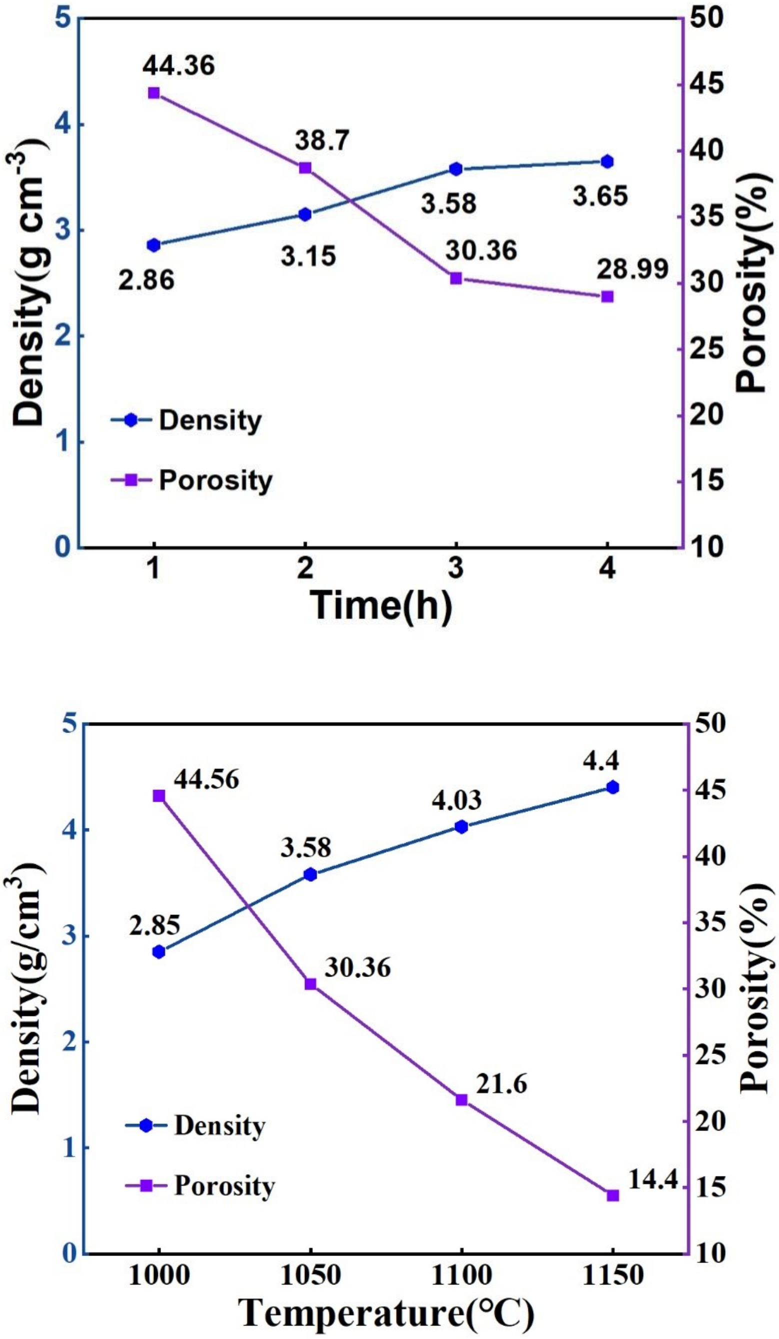

Figure S5. Variation of framework density and porosity with sintering time and temperature.

The density was calculated from pellets with a diameter of 10 mm based on mass and volume, while subsequent porosity measurements were performed using pellets with a diameter of 18 mm.

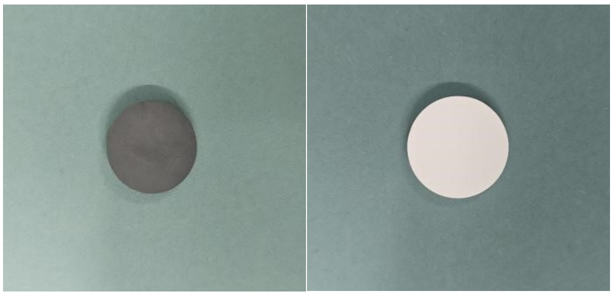

Figure S6. Optical photographs of ceramic bodies.

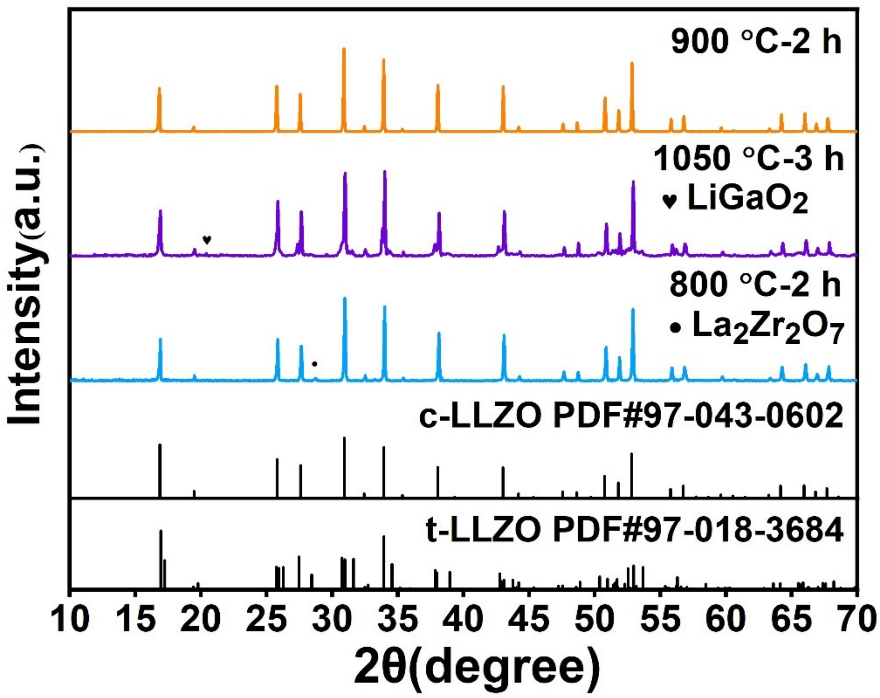

Figure S7. Phase evolution of the framework during the preparation process.

During the high-temperature sintering process of LLZO ceramics, significant volatilization of lithium results in a decrease in lithium-ion concentration within the lattice. This leads to the formation of enriched Li_2O liquid phases at grain boundaries. Upon cooling, these liquid phases react with the doped Ga_2O_3 to form $LiGaO_2$. Concurrently, if the precursor reaction is incomplete, $La_2Zr_2O_7$ phases may remain. The presence of these secondary phases severely impedes lithium-ion transport: the discontinuous distribution of $LiGaO_2$ disrupts the continuity of grain boundary conduction, while the non-lithium-ion-conducting $La_2Zr_2O_7$ directly blocks transport pathways. Collectively, these effects increase grain boundary impedance and reduce overall ionic conductivity. However, subsequent heat treatment eliminates these metastable secondary phases. $LiGaO_2$ decomposes to provide a lithium source, while $La_2Zr_2O_7$ reacts with this lithium source and reintegrates into the lattice, ultimately transforming into pure cubic LLZO.

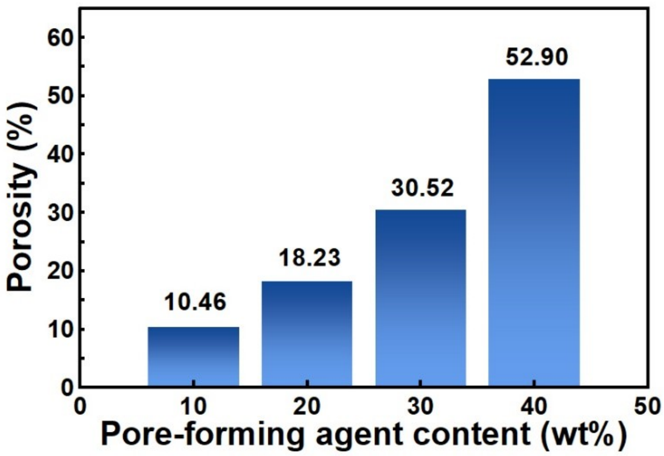

Figure S8. Variation of porosity with pore-forming agent content.

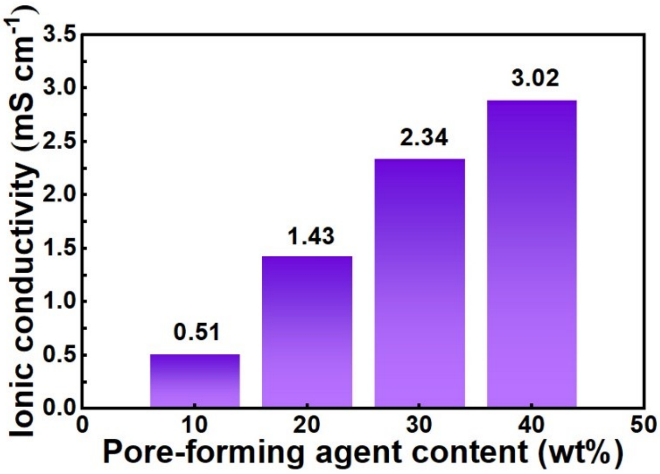

Figure S9. Variation of ionic conductivity with pore-forming agent content.

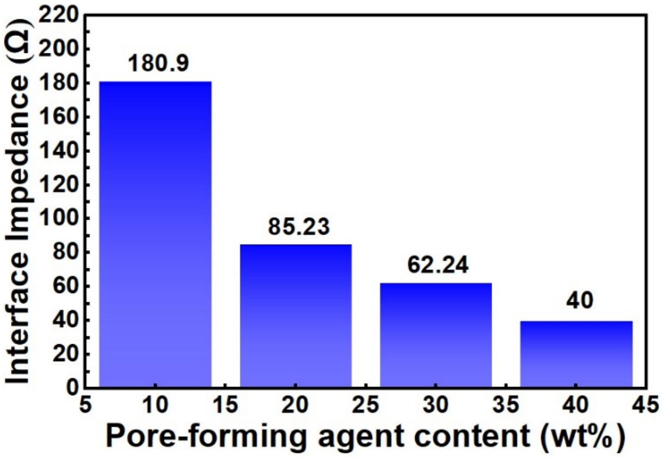

Figure S10. Variation of interfacial impedance with pore-forming agent content.

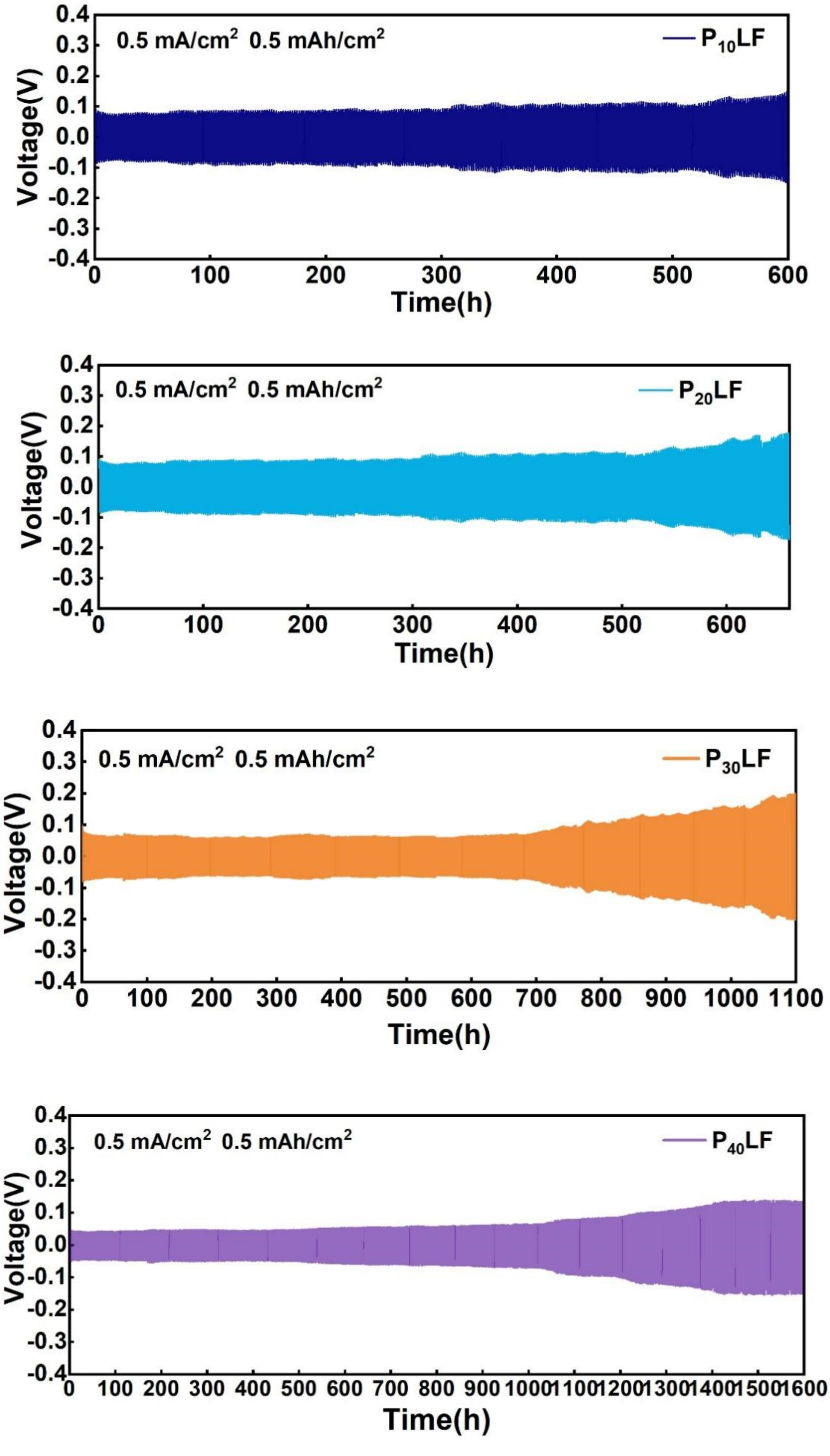

Figure S11. Long-term cycling performance of Li/PLF-$LiPF_6$/Li cells at 25 °C under a current density of 0.5 mA cm^{-2}.

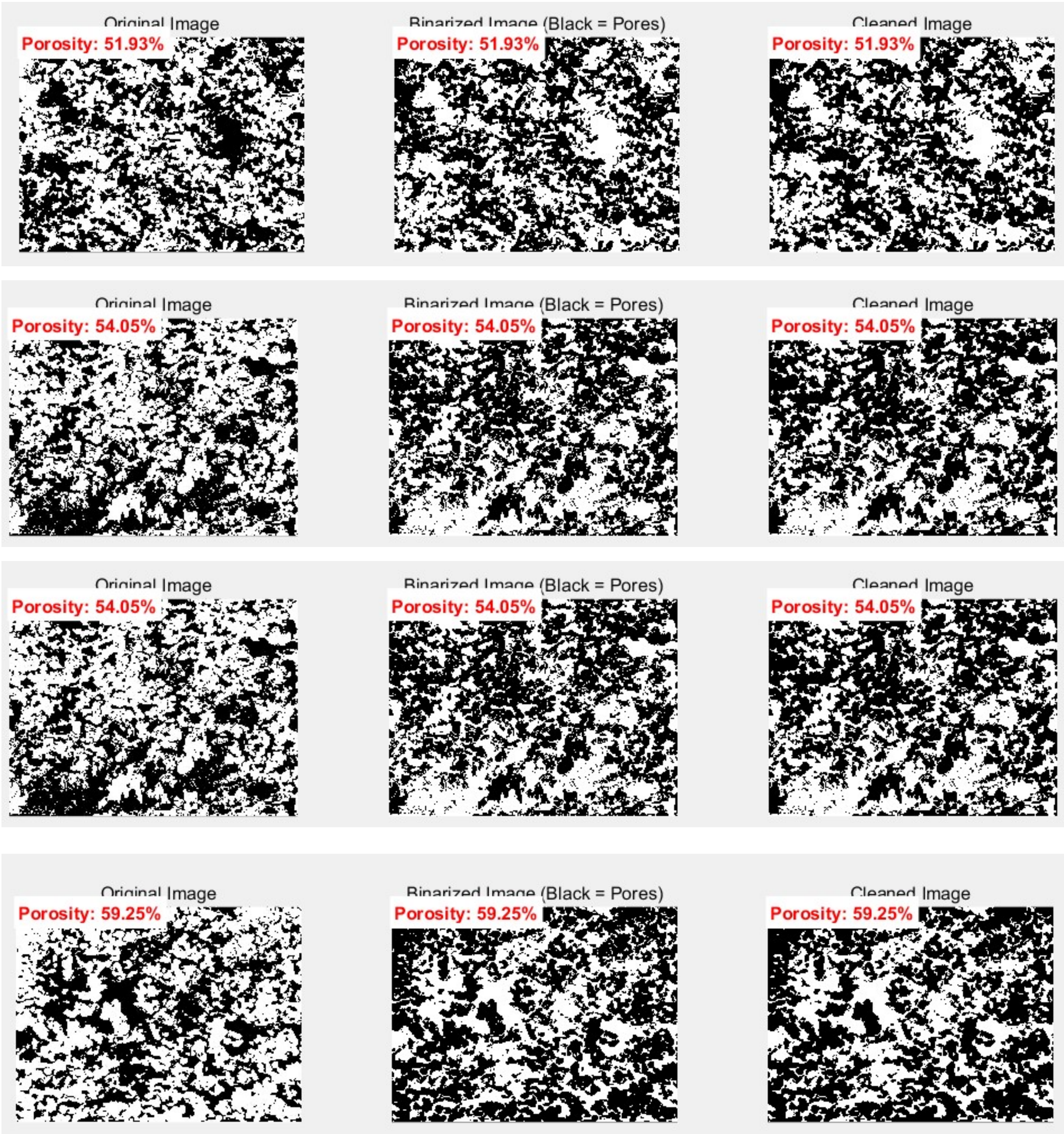

Figure S12. Pore analysis of SEM-imaged specimens

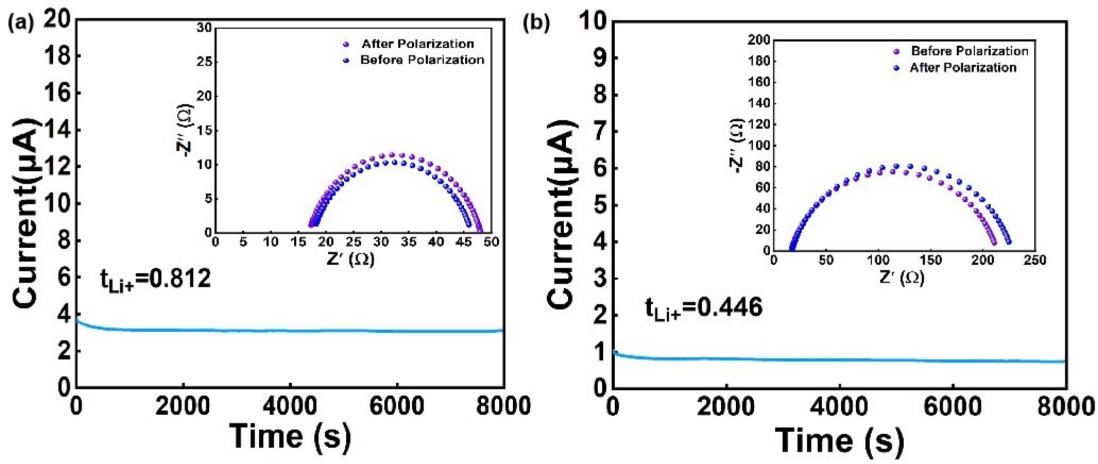

Figure S13. Comparison of lithium ion mobility between Li/ P_GLF-$LiPF_6$/Li and Li/ SiO_2 -$LiPF_6$/Li symmetric cells.

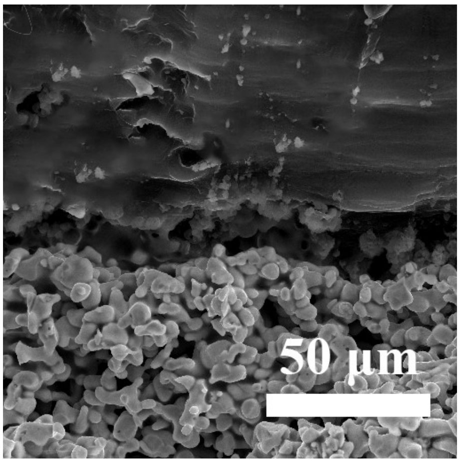

Figure S14. SEM image of the anode–framework interface after 100 cycles at 1 C.

The battery was disassembled after 100 cycles at 1 C, followed by vacuum drying at 40 °C for 24 h, and the electrode–electrolyte interface was then examined using SEM.

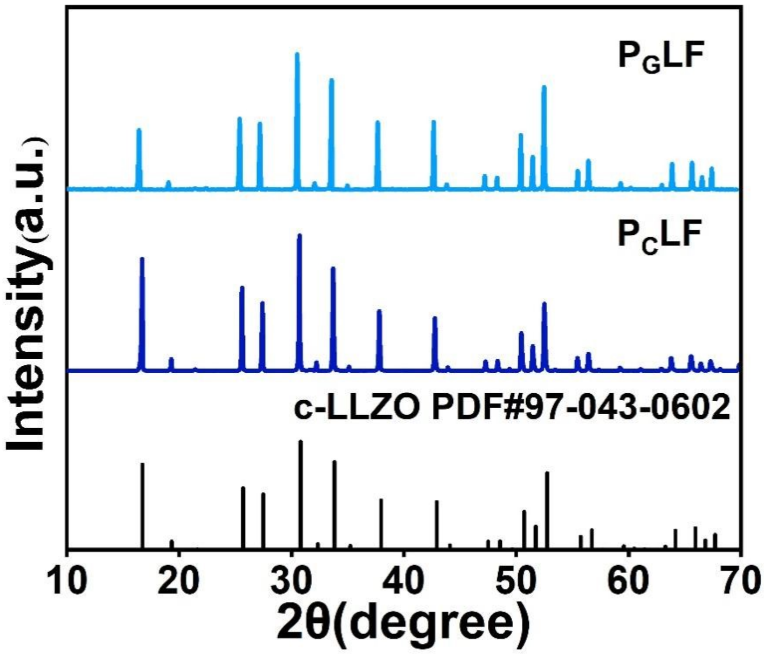

Figure S15. Phase structures of P_GLF and P_CLF.

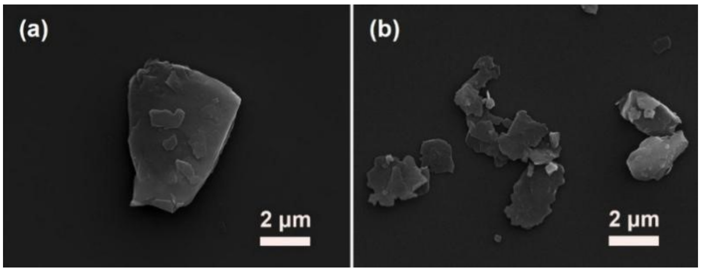

Figure S16. (a) Graphite and (b) Charcoal Microstructure

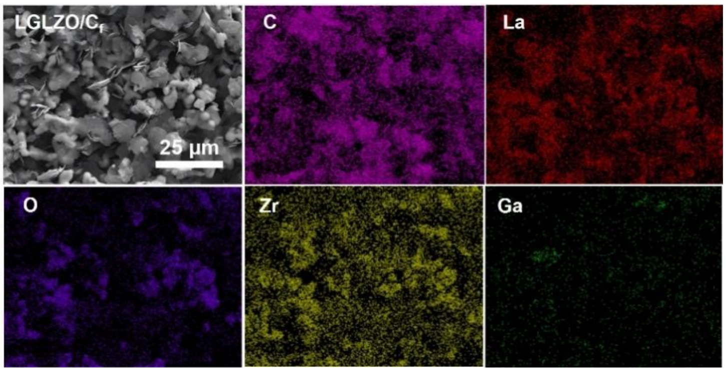

Figure S17. EDS of LGLZO/C_f composite powder

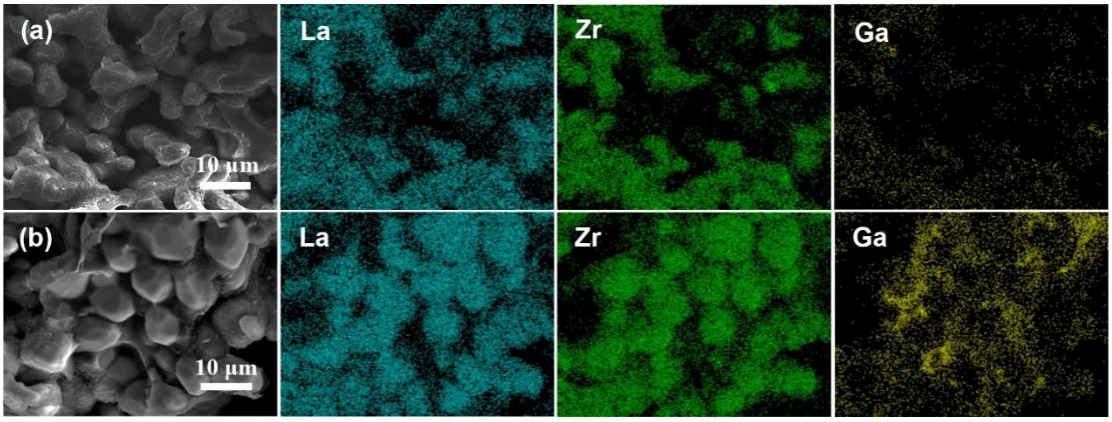

Figure S18. SEM images and EDS spectra of (a) P_GLF and (b) P_CLF.

Table S1. Porosity in Quasi-Solid Electrolyte article

Title	Porosity	Ref.
Garnet-Based Solid-State Li Batteries with High-Surface-Area Porous LLZO Membranes (ACS Applied Materials & Interfaces, 2024).	51%	[S1]
Oriented porous LLZO 3D structures obtained by freeze casting for battery applications (Journal of Materials Chemistry A, 2019)	60%	[S2]
Uniformly porous PVDF-co-HFP membranes prepared by mixed solvent phase separation for direct contact membrane distillation（Journal of Membrane Science，2024）	86%	[S3]
Self-adaptable gel polymer electrolytes enable high-performance and all-round safety lithium ion batteries（Energy Storage Materials，2022）	78%	[S4]
Poly(vinylidene fluoride)/SiO_2 composite membranes prepared by electrospinning and their excellent properties for nonwoven separators for lithium-ion batteries（Journal of Power Sources，2014）	75%	[S5]

Table S2. Changes in the Quality with Different Carbon Content

Content of perforating agent	Organization	Before calcination	After calcination	Variation in Mass Before and After
10 %	Quality (g)	1.0942	0.9615	-11.13 %
20 %	Quality (g)	1.2244	0.9545	-22.04 %
30 %	Quality (g)	1.1303	0.7700	-31.87 %
40 %	Quality (g)	1.0392	0.6306	-39.32 %

Table S3. Comparison of ionic conductivity, current density, and cycling stability of this work with previously reported electrolytes.

Electrolyte	Ionic conductivity ($\times 10^{-3}$ S cm^{-1})	Current density (mA cm^{-2})	Cycle Time (h)	Ref.
PEO/LLZO	1.36	0.2	400	[S6]
PEO/LLZO framework	0.14	0.2	400	[S7]
LE/LLZO framework	4.2	0.5	1400	[S8]
PEO/LLZO nanowires	1.53	0.5	1050	[S9]
PVDF/LLZTO	0.12	0.1	1200	[S10]
PEO/LICGC	0.29	0.2	800	[S11]
PEO/Li_2ZrO_3	0.5	0.1	200	[S12]
LE/FEC/LLZTO	0.65	0.1	500	[S13]
PVDF/TiO_2	0.33	0.2	3800	[S14]
LE/MOFs	0.24	0.5	1000	[S15]
LE/MOFs	7.74	0.2	1000	[S16]
LE/LATP framework	7.9	1	120	[S17]
PEO/LLZTO	0.22	0.1	2500	[S18]
PEO/LLZO	0.18	0.5	200	[S19]
PEO/LLZO	0.64	0.2	600	[S20]
PEO/$Bi_4Ti_3O_{12}$	0.62	0.1	3000	[S21]
LE/ODA nanofiber	2.9	1	2000	[S22]
LE/PIM-$CONH_2$	1.08	0.1	1500	[S23]
LE/LLZO framework	2.06	0.5	800	[S24]
LE/LLZO-TiO_2	1.6	0.3	500	[S25]

LE/LGLZO framework	2.54	0.5	1150	This work
LE/LGLZO framework	3.02	0.5	1600	This work

Reference

[S1] Zhang, H., Okur, F., Pant, B., Klimpel, M., et al. Garnet-based solid-state Li batteries with high-surface-area porous LLZO membranes. ACS Applied Materials & Interfaces, 2024, 16(10), 12353-12362.

[S2] Shen H, Yi E, Amores M, et al. Oriented porous LLZO 3D structures obtained by freeze casting for battery applications[J]. Journal of materials chemistry A, 2019, 7(36): 20861-20870.

[S3] Al Nuaimi, R., Thankamony, R. L., et al. Uniformly porous PVDF-co-HFP membranes prepared by mixed solvent phase separation for direct contact membrane distillation. Journal of Membrane Science, 2024, 711, 123175.

[S4] Long, M. C., Wu, G., Wang, X. L., et al. Self-adaptable gel polymer electrolytes enable high-performance and all-round safety lithium ion batteries. Energy Storage Materials, 2022, 53, 62-71.

[S5] Zhang F, Ma X, Cao C, et al. Poly (vinylidene fluoride)/SiO2 composite membranes prepared by electrospinning and their excellent properties for nonwoven separators for lithium-ion batteries[J]. Journal of Power Sources, 2014, 251: 423-431.

[S6] Yin J, Xu X, Jiang S, et al. High ionic conductivity PEO-based electrolyte with 3D framework for Dendrite-free solid-state lithium metal batteries at ambient temperature[J]. Chemical Engineering Journal, 2022, 431: 133352.

[S7] Zhang H, An X, Lu Z, et al. A three dimensional interconnected $Li_7La_3Zr_2O_{12}$ framework composite solid electrolyte utilizing lignosulfonate/cellulose nanofiber bio-template for high performance lithium ion batteries[J]. Journal of Power Sources, 2020, 477: 228752.

[S8] Wang Z, Chen L, Niu C, et al. Synthesis of Quasi-Solid Electrolytes from High-Strength and Highly Oriented LLZO Porous Ceramics[J]. ACS Applied Energy Materials, 2024, 7(21): 9670-9675.

[S9] Wan Z, Lei D, Yang W, et al. Low resistance‐integrated all‐solid‐state battery achieved by $Li_7La_3Zr_2O_{12}$ nanowire upgrading polyethylene oxide (PEO) composite electrolyte and PEO cathode binder[J]. Advanced Functional Materials, 2019, 29(1): 1805301.

[S10] Ma X, Mao D, Xin W, et al. Flexible Composite Electrolyte Membranes with Fast Ion Transport Channels for Solid-State Lithium Batteries[J]. Polymers, 2024, 16(5): 565.

[S11] Sahore R, Armstrong B L, Tang X, et al. Role of Scaffold Architecture and Excess Surface Polymer Layers in a 3D‐Interconnected Ceramic/Polymer Composite Electrolyte[J]. Advanced Energy Materials, 2023, 13(19): 2203663.

[S12] Yang L, Zhang H, Xia E, et al. PEO/Li_2ZrO_3 composite electrolyte for solid-state rechargeable lithium battery[J]. Journal of Energy Storage, 2023, 65: 107283.

[S13] Cai D, Zhang J, Li F, et al. LLZTO Nanoparticle-and Cellulose Mesh-Coreinforced Flexible Composite Electrolyte for Stable Li Metal Batteries[J]. ACS Applied Materials & Interfaces, 2023, 15(31): 37884-37892.

[S14] Chen S, Guo J, Zang H, et al. Oxygen vacancy-enriched TiO_2 nanosheets filled PVDF electrolyte for semi-solid-state batteries: Synergistic effects of conformational transition and defect sites[J]. Journal of Alloys and Compounds, 2025, 1020: 179357.

[S15] Nguyen M H, Ngo N M, Kim B K, et al. Dual Ionic Pathways in Semi‐Solid Electrolyte based on Binary Metal‐Organic Frameworks Enable Stable Operation of Li‐Metal Batteries at Extremely High Temperatures[J]. Advanced Science, 2024, 11(43): 2407018.

[S16] Tao F, Wang X, Jin S, et al. A composite of hierarchical porous MOFs and halloysite nanotubes as single‐ion‐conducting electrolyte toward high‐performance solid‐state lithium‐ion batteries[J]. Advanced Materials, 2023, 35(29): 2300687.

[S17] Reinoso D M, de la Torre-Gamarra C, Fernández-Ropero A J, et al. Advancements in quasi-solid-state Li batteries: a rigid hybrid electrolyte using

LATP porous ceramic membrane and infiltrated ionic liquid[J]. ACS Applied Energy Materials, 2024, 7(4): 1527-1538.

[S18] Li X, Liu S, Shi J, et al. High performance porous poly (ethylene oxide)-based composite solid electrolytes[J]. Chemical Engineering Journal, 2023, 468: 143795.

[S19] Hu W, Chien P H, Wu N, et al. High Li+ Conducting Porous Garnet Enables Fast Li+ Conduction in Polymer/Garnet Composite Electrolyte[J]. ACS Applied Energy Materials, 2024, 7(18): 8077-8084.

[S20] Xie Y, Huang L, Chen Y. A porous garnet $Li_7La_3Zr_2O_{12}$ scaffold with interfacial modification for enhancing ionic conductivity in PEO-based composite electrolyte[J]. Journal of Membrane Science, 2023, 683: 121784.

[S21] Kang J, Yan Z, Gao L, et al. Improved ionic conductivity and enhancedinterfacial stability of solid polymer electrolytes with porous ferroelectric ceramic nanofibers[J]. Energy Storage Materials, 2022, 53: 192-203.

[S22] Huang Y, Liu S, Chen Q, et al. Constructing highly conductive and thermomechanical stable quasi‐solid electrolytes by self‐polymerization of liquid electrolytes within porous polyimide nanofiber films[J]. Advanced Functional Materials, 2022, 32(31): 2201496.

[S23] Lu S, He K, Zhou L, et al. The Regulation of Ion Transport Microenvironment in Micropores to Precisely Construct Porous Polymer Electrolytes for Solid-State Lithium–Metal Batteries[J]. ACS nano, 2025.

[S24] Zhou Y, Tian Y, Wang W, et al. Porous $Ga_{0.25}Li_{6.25}La_3Zr_2O_{12}$ frameworks by gelcasting–reaction sintering for high-performance hybrid quasi-solid lithium metal batteries[J]. Journal of Materials Chemistry A, 2023, 11(44): 23932-23939

[S25] Luo P, Zeng B, Li W, et al. TiO_2‐Induced Conversion Reaction Eliminating Li_2CO_3 and Pores/Voids Inside Garnet Electrolyte for Lithium‐Metal Batteries[J]. Advanced Functional Materials, 2023, 33(35): 2302299.